

# Precision growth index using the clustering of cosmic structures and growth data

---

**Athina Pouri<sup>a,b</sup>, Spyros Basilakos<sup>a</sup>, Manolis Plionis<sup>c,d,e</sup>**

<sup>a</sup> *Academy of Athens, Research Center for Astronomy and Applied Mathematics, Soranou Efessiou 4, 11527, Athens, Greece*

<sup>b</sup> *Faculty of Physics, Department of Astrophysics - Astronomy - Mechanics, University of Athens, Panepistemiopolis, Athens 157 83*

<sup>c</sup> *Physics Dept., Sector of Astrophysics, Astronomy & Mechanics, Aristotle Univ. of Thessaloniki, Thessaloniki 54124, Greece*

<sup>d</sup> *Instituto Nacional de Astrofísica Óptica y Electrónica, 72000 Puebla, México*

<sup>e</sup> *IAASARS, National Observatory of Athens, P.Pendeli 15236, Greece*

*E-Mails: athpouri@phys.uoa.gr, svasil@academyofathens.gr, mplionis@auth*

**ABSTRACT:** We use the clustering properties of Luminous Red Galaxies (LRGs) and the growth rate data provided by the various galaxy surveys in order to constrain the growth index ( $\gamma$ ) of the linear matter fluctuations. We perform a standard  $\chi^2$ -minimization procedure between theoretical expectations and data, followed by a joint likelihood analysis and we find a value of  $\gamma = 0.56 \pm 0.05$ , perfectly consistent with the expectations of the  $\Lambda$ CDM model, and  $\Omega_{m0} = 0.29 \pm 0.01$ , in very good agreement with the latest Planck results. Our analysis provides significantly more stringent growth index constraints with respect to previous studies, as indicated by the fact that the corresponding uncertainty is only  $\sim 0.09\gamma$ . Finally, allowing  $\gamma$  to vary with redshift in two manners (Taylor expansion around  $z = 0$ , and Taylor expansion around the scale factor), we find that the combined statistical analysis between our clustering and literature growth data alleviates the degeneracy and obtain more stringent constraints with respect to other recent studies.

**KEYWORDS:** Large scale structure, dark energy, linear growth.

---

## Contents

|   |           |
|---|-----------|
| <b>1. Introduction</b>  | <b>1</b>  |
| <b>2. Angular Correlation Function Data and Growth data</b>           | <b>2</b>  |
| <b>3. Modeling the Theoretical Correlation Function</b>               | <b>4</b>  |
| 3.1 The linear growth factor $D(a)$ and the linear growth rate $f(a)$ | 5         |
| 3.2 The evolution of linear bias, $b(z)$                              | 6         |
| 3.3 CDM Power Spectrum, $P(k)$  | 7         |
| <b>4. Fitting Theoretical Models to the data</b>                      | <b>8</b>  |
| 4.1 Constraints on $(\Omega_{m0}, \gamma)$                            | 11        |
| 4.2 Constraints on $\gamma(z)$  | 14        |
| 4.3 Using the priors provided by the Planck team                      | 15        |
| <b>5. Conclusions</b>   | <b>16</b> |

---

## 1. Introduction

The statistical analysis of various cosmological data (SNIa, Cosmic Microwave Background-CMB, Baryonic Acoustic Oscillations-BAOs, Hubble parameter measurements etc) strongly suggests that we live in a spatially flat universe that consists of  $\sim 4\%$  baryonic matter,  $\sim 26\%$  dark matter and  $\sim 70\%$  some sort of dark energy (hereafter DE) which is necessary to explain the accelerated expansion of the universe (cf. [1, 2, 3, 4, 5, 6, 7] and references therein). Although there is a common agreement regarding the ingredients of the universe, there are different views concerning the possible physical mechanism which is responsible for the cosmic acceleration. Briefly, the general path that one can follow in order to mathematically treat the accelerated expansion of the universe is to see DE either as a new field in nature or as a modification of General Relativity (see for review [8, 9, 10]).

An interesting approach to discriminate between scalar field DE and modified gravity is to use the evolution of the linear growth of matter perturbations  $\delta_m(z) = \delta\rho_m/\rho_m$  [11, 12, 13]. Specifically, a useful tool in this kind of studies is the so called growth rate of clustering, which is defined as  $f(a) = \frac{d\ln D}{d\ln a} \simeq \Omega_m^\gamma(a)$ , where  $a(z) = (1+z)^{-1}$  is the scale factor of the universe,  $\Omega_m(a)$  is the dimensionless matter density parameter,  $\gamma$  is the growth index and  $D(a) = \delta_m(a)/\delta_m(a=1)$  is the linear growth factor scaled to unity at the present time [14, 15]. The accurate determination of the growth index is considered one of the main goals of Observational Cosmology because it can be used in order to check the validity of General Relativity on cosmological scales. The basic ingredient in this approach comes from the fact that  $\gamma$  depends weakly on the dark energy equation of state (hereafter EoS) parameter  $w(z)$  [12], implying that one can split the background expansion history,  $H(z)$ , constrained by geometric probes (SNIa, BAO, CMB), from the dynamical perturbations growth history.

Theoretically speaking, it has been shown that for those DE models which are within the framework of GR and have a constant EoS parameter, the growth index  $\gamma$  is well approximated by  $\gamma \simeq \frac{3(w-1)}{6w-5}$  [12, 16, 15, 17]. In the case of the concordance  $\Lambda$ CDM model ( $w(z) = -1$ ) the above formula reduces to  $\gamma \approx 6/11$ . Considering the braneworld model of [18] we have  $\gamma \approx 11/16$  (see [12, 19, 20, 21]). Finally, for some  $f(R)$  gravity models it has been found that  $\gamma \simeq 0.415 - 0.21z$  for various parameter values (see [22, 23]), while for the Finsler-Randers cosmology, Basilakos & Stavrinos [24] found  $\gamma \approx 9/14$ .

From the large scale structure point of view, the study of the distribution of matter on large scales using different extragalactic mass tracers (galaxies, AGNs, clusters of galaxies etc) provides important constraints on structure formation theories. In particular, since gravity reflects, via gravitational instability, on the nature of clustering [14] it has been proposed to use the clustering/biasing properties of the mass tracers in constraining cosmological models (see [25, 26, 27, 28]) as well as to test the validity of GR on extragalactic scales ([29] for a recent review see [30]).

Based on the above arguments, the aim of the current study is to place constraints on the  $(\Omega_m, \gamma)$  parameter space using the measured two-point angular correlation function (hereafter ACF) of the LRGs, with known redshift distribution. The basic idea is to compare the measured and the theoretically predicted ACF, which is based on the 3D power spectrum, the evolution of the relevant bias parameter and the Limber's inversion integral equation. Therefore, the predicted theoretical ACF depends also on the growth of linear matter perturbations via which the  $(\Omega_m, \gamma)$  pair, which can thus be constrained. The merit of utilizing ACF data for such a task is related to the fact that we do not need to consider a fiducial cosmological model in order to derive the ACF data, as well as on the fact that the ACF is unaffected by redshift-space distortions. In addition to ACF, we use the recent growth rate data as collected by Nesseris & Garcia-Bellido [31], Hudson & Turnbull [32], Beutler et al. [33] and Basilakos et al. [57] in order to put tight constraints on  $(\Omega_m, \gamma)$ .

The structure of the paper is as follows. In section 2 we present the angular correlation function data, measured for LRGs and the growth data. In section 3 we discuss the theoretical angular correlation function model and basic ingredients in order to calculate it, such as the linear growth of matter perturbations, the evolution of the linear bias factor and the CDM power spectrum. The details of our methodology used to fit models to the data and our results are presented in section 4, while our main conclusions in section 5.

## 2. Angular Correlation Function Data and Growth data

It is well known that the two-point ACF,  $w(\theta)$ , is defined as the excess joint probability over random of finding two mass tracers (galaxies, AGNs, clusters) separated by an angular separation  $\theta$ . Therefore by definition we have  $w(\theta) = 0$  for a random distribution of sources. In this work we use the ACF of 2SLAQ LRGs galaxies with median redshift  $z_\star \simeq 0.55$ . In particular, we utilize the ACF of 655775 photometrically selected LRGs from the SDSS DR5 catalogue, already estimated in [35]. This sample has been compiled using the same selection criteria as the 2dF-SDSS LRG and Quasar survey (hereafter 2SLAQ), which covers the redshift range:  $0.45 < z < 0.8$ . Following the original paper of [35] we use the ACF up to an angular scale of  $6000''$  in order to avoid the effects of BAO's. Since the aim of our paper is to put constraints on the linear growth index we also exclude small angular scales ( $\theta < 120''$ , which corresponds to  $\leq 0.6 h^{-1}$  Mpc at  $z_\star$ ) where strong non-linear effects (the

**Table 1:** The measured angular correlation function data of the 2SLAQ LRGs from [35]. We use here bootstrap errors meaning that we need to multiply the uncertainties of [35] with  $\sqrt{3}$ .

| Index | $\theta''$ | $w(\theta)$ | $\delta w(\theta)$ |
|-------|------------|-------------|--------------------|
| 1     | 153.72     | 0.285       | 0.0061             |
| 2     | 230.64     | 0.199       | 0.0038             |
| 3     | 345.96     | 0.152       | 0.0026             |
| 4     | 518.94     | 0.113       | 0.0019             |
| 5     | 778.2      | 0.078       | 0.0018             |
| 6     | 1167.6     | 0.055       | 0.0012             |
| 7     | 1751.4     | 0.038       | 0.0011             |
| 8     | 2626.8     | 0.0226      | 0.0009             |
| 9     | 3600       | 0.0144      | 0.0008             |
| 10    | 4800       | 0.0086      | 0.00076            |
| 11    | 6000       | 0.0054      | 0.00067            |

so-called “one-halo” term) are expected, although we do use in our theoretical modeling a mildly non-linear correction term (see also section 3.3). In Table I we list the precise numerical values of the ACF data points with the corresponding errors that are used in our analysis.

In addition, we utilize in our analysis the growth rate of clustering data which are based on the PSCz, 2dF, VVDS, SDSS, 6dF, 2MASS, BOSS and *WiggleZ* galaxy surveys, for which their combination parameter of the growth rate of structure,  $f(z)$ , and the redshift-dependent rms fluctuations of the linear density field,  $\sigma_8(z)$ , is available as a function of redshift,  $f(z)\sigma_8(z)$ . The total sample contains 16 entries (as collected by Basilakos et al. [57]). The  $f\sigma_8$  estimator is almost a model-independent way of expressing the observed growth history of the universe (see [36]). Indeed the observed growth rate of structure ( $f_{obs} = \beta b$ ) is derived from the redshift space distortion parameter  $\beta(z)$  and the linear bias. Observationally, using the anisotropy of the spatial correlation function one can estimate the  $\beta(z)$  parameter (see also section 3.2). On the other hand, the linear bias factor can be defined as the ratio of the variances of the tracer (galaxies, QSOs etc) and underlying mass density fields, smoothed at  $8h^{-1}$  Mpc  $b(z) = \sigma_{8,tr}(z)/\sigma_8(z)$ , where  $\sigma_{8,tr}(z)$  is measured directly from the sample. Combining the above definitions we arrive at  $f\sigma_8 = \beta\sigma_{8,tr}$ . Since different authors have estimated  $f\sigma_8$  using different cosmologies, we need to convert them to the same cosmological background in order to be able to utilize them consistently. Specifically, we wish to translate the value of growth data  $f\sigma_8$  from a reference cosmological model, say Ref, to the background cosmology. The definition of  $f(z) \simeq \Omega_m(z)^{\gamma(z)}$  and  $\sigma_8(z) = \sigma_8 D(\Omega_{m0}, z)$  (for more details see section 3.1) simply implies a correction factor:

$$C_f = \frac{f\sigma_{8,obs}}{f\sigma_{8,obs}^{Ref}} = \left[ \frac{\Omega_m(z)}{\Omega_m^{Ref}(z)} \right]^{\gamma(z)} \frac{\sigma_8 D(\Omega_{m0}, z)}{\sigma_8^{Ref} D(\Omega_{m0}^{Ref}, z)}. \quad (2.1)$$

Notice that the  $f\sigma_{8,obs}^{Ref}$  data and the corresponding uncertainties can be found in Table I of [57].

### 3. Modeling the Theoretical Correlation Function

In this section we briefly discuss the basic steps of modeling the theoretically expected ACF for the two different mass tracers used and of the evolution of bias of extragalactic mass tracers. Considering a spatially flat Friedmann-Lemaître-Robertson-Walker (FLRW) geometry), we can easily relate via the Limber's inversion equation the ACF with the two point spatial correlation function  $\xi(r, z)$ :

$$w(\theta) = 2 \frac{H_0}{c} \int_0^\infty \left( \frac{1}{N} \frac{dN}{dz} \right)^2 E(z) dz \int_0^\infty \xi(r, z) du, \quad (3.1)$$

where  $1/N dN/dz$  is the normalized redshift distribution of the sources under study, which is provided by a random subsample of the source population for which redshifts (spectroscopic or photometric) are available (see section 4).

The spatial correlation function of the mass tracers is given by

$$\xi(r, z) = b^2(z) \xi_{DM}(r, z) \quad (3.2)$$

where  $b(z)$  is the evolution of the linear bias, and  $\xi_{DM}$  is the corresponding correlation function of the underlying mass distribution which is written as

$$\xi_{DM}(r, z) = \frac{1}{2\pi^2} \int_0^\infty k^2 P(k, z) \frac{\sin(kr/a)}{(kr/a)} dk. \quad (3.3)$$

with  $P(k, z) = D^2(z)P(k)$ , and  $P(k)$  denoting the power spectrum of the matter fluctuations.

The variable  $r$  corresponds to the physical separation between two sources having an angular separation,  $\theta$  (in steradians). In the case of a small angle approximation the physical separation becomes

$$r \simeq a(z) (u^2 + x^2 \theta^2)^{1/2} \quad (3.4)$$

where  $u$  is the line-of-sight separation of any two sources and  $x(z)$  is the comoving distance, given by:

$$x(z) = \frac{c}{H_0} \int_0^z \frac{dy}{E(y)}, \quad (3.5)$$

$E(z) = H(z)/H_0$ , is the normalized Hubble parameter.

Inserting Eqs.(3.2), (3.3), (3.4) and  $a(z) = 1/(1+z)$  into Eq.(3.1) and integrating over the variable  $u$  we arrive at (see also [37]) our final theoretically expected ACF:

$$w(\theta) = \frac{1}{2\pi} \int_0^\infty k^2 P(k) dk \int_0^\infty D^2(z) j(k, z, \theta) dz \quad (3.6)$$

with

$$j(k, z, \theta) = \frac{H_0}{c} \left( \frac{1}{N} \frac{dN}{dz} \right)^2 b^2(z) E(z) J_0(k \theta x(z)) \quad (3.7)$$

where  $J_0$  is the Bessel function of zero kind, given by:

$$J_0(\omega) = \frac{2}{\pi} \int_0^\infty \sin(\omega \cosh \tau) d\tau = \frac{1}{\pi} \int_0^\pi \cos(\omega \sin \tau) d\tau \quad (3.8)$$

Note that the expectations for the different mass tracers enter through the bias evolution factor,  $b(z)$ , and the tracer redshift distribution  $1/N dN/dz$ .

Obviously, the dependence of ACF on gravity as well as on the different expansion models enters through the behavior of  $D(z)$ , which in turn depends on  $\gamma$  (see equation 3.15), and on  $E(z) = H(z)/H_0$  respectively. In the subsections below we present the different ingredients that enter in Eq.(3.6), namely, the linear perturbation growth rate, the bias evolution factor and the CDM power spectrum.

### 3.1 The linear growth factor $D(a)$ and the linear growth rate $f(a)$

Here we provide the form of the linear density perturbation growth rate, which is the ingredient through which the growth index,  $\gamma$ , enters in our analysis.

At sub-horizon scales the basic differential equation which describes the linear matter fluctuations ([11, 12, 38, 39, 40, 41] and references therein) is

$$\ddot{\delta}_m + 2H\dot{\delta}_m = 4\pi G_{\text{eff}}\rho_m\delta_m \quad (3.9)$$

where  $\rho_m \propto a^{-3}$  is the matter density,  $G_{\text{eff}} = G_N Q(t)$  with  $G_N$  being the Newton's gravitational constant and the function  $Q(t)$  depends on gravity. For the scalar field DE models,  $G_{\text{eff}}$  is equal to  $G_N$ , i.e.,  $Q(a) = 1$ , while for the case of modified gravity models we have  $Q(a) \neq 1$  and subsequently  $G_{\text{eff}} \neq G_N$ .

The growing-mode solution of equation (3.9) is  $\delta_m \propto D(a)$ , where  $D(a)$  is the linear growing mode usually scaled to unity at the present time. Generally, for either modified gravity or scalar field DE we can write the following useful parametrization [14, 15, 12]

$$f(a) = \frac{d\ln\delta_m}{d\ln a} \simeq \Omega_m^\gamma(a) \quad (3.10)$$

where  $\Omega_m(a) = \Omega_{m0}a^{-3}/E^2(a)$ . Therefore, using  $d/dt = H d/d\ln a$  we express Eq.(3.9) in terms of  $f(a)$  as:

$$\frac{df}{d\ln a} + f^2 + \left( \frac{\dot{H}}{H^2} + 2 \right) f = \frac{3}{2}Q(a)\Omega_m(a) \quad (3.11)$$

where for the  $\Lambda$ CDM expansion we have

$$\frac{\dot{H}}{H^2} + 2 = \frac{1}{2} - \frac{3}{2}w(a)[1 - \Omega_m(a)] \quad (3.12)$$

and  $w(a) = -Q(a) = -1$ . In this case the normalized Hubble parameter  $E(a)$ , is:

$$E(a) = (\Omega_{m0}a^{-3} + \Omega_{\Lambda0})^{1/2} \quad (3.13)$$

with  $\Omega_{\Lambda0} = 1 - \Omega_{m0}$  and  $H_0$  the Hubble constant<sup>1</sup>. As we have stated in the introduction we can separate the background expansion  $H(a)$  from the growth history [12].

The parametrization of Eq.(3.10) greatly simplifies the numerical calculations of Eq.(3.9). Indeed, providing a direct integration of Eq.(3.10) we easily find

$$\delta_m(a, \gamma) = a(z) \exp \left[ \int_{a_i}^{a(z)} \frac{dy}{y} (\Omega_m^\gamma(y) - 1) \right] \quad (3.14)$$

---

<sup>1</sup>For the comoving distance and for the dark matter halo mass we use the traditional parametrization  $H_0 = 100h\text{km/s/Mpc}$ . Of course, when we treat the power spectrum shape parameter  $\Gamma$  we utilize  $h \equiv \bar{h} = 0.68$  [7].

where  $a_i$  is the scale factor of the universe at which the matter component dominates the cosmic fluid (here we use  $a_i \simeq 10^{-2}$ ). Then the linear growth factor, normalized to unity at the present epoch, is:

$$D(a) = \frac{\delta_m(a, \gamma)}{\delta_m(1, \gamma)} = \frac{a(z) \exp \left[ \int_{a_i}^{a(z)} \frac{dy}{y} (\Omega_m^\gamma(y) - 1) \right]}{\exp \left[ \int_{a_i}^1 \frac{dy}{y} (\Omega_m^\gamma(y) - 1) \right]}. \quad (3.15)$$

However,  $\gamma$  may not be a constant but rather evolve with redshift;  $\gamma \equiv \gamma(z)$ . In such a case, inserting Eq.(3.10) into Eq.(3.11) we obtain:

$$-(1+z)\gamma' \ln(\Omega_m) + \Omega_m^\gamma + 3w(1 - \Omega_m) \left( \gamma - \frac{1}{2} \right) + \frac{1}{2} = \frac{3}{2} Q \Omega_m^{1-\gamma}$$

where the prime denotes derivative with respect to redshift. Various functional forms of  $\gamma(z)$  have been proposed in the literature [42, 43, 44, 45], for example:

$$\gamma(z) = \begin{cases} \gamma_0 + \gamma_1 z, & \Gamma_1\text{-parametrization} \\ \gamma_0 + \gamma_1 z/(1+z), & \Gamma_2\text{-parametrization.} \end{cases} \quad (3.16)$$

Using the above parametrizations and Eq.(3.1) evaluated at the present time ( $z = 0$ ), one can easily obtain the parameter  $\gamma_1$  in terms of  $\gamma_0$

$$\gamma_1 = \frac{\Omega_{m0}^{\gamma_0} + 3w_0(\gamma_0 - \frac{1}{2})(1 - \Omega_{m0}) - \frac{3}{2}Q_0\Omega_{m0}^{1-\gamma_0} + \frac{1}{2}}{\ln \Omega_{m0}}. \quad (3.17)$$

Owing to the fact that the  $\Gamma_1$  parametrization is valid only at relatively low redshifts ( $0 \leq z \leq 0.5$ ), for  $z > 0.5$  we utilize  $\gamma = \gamma_0 + 0.5\gamma_1$ . As an example, in the case of the usual  $\Lambda$ CDM cosmological model (ie.,  $Q_0 = 1$ ,  $w_0 = -1$  and  $\gamma_0^{(th)} \simeq 6/11$ ) with  $\Omega_{m0} = 0.30$ , Eq.(3.17) gives  $\gamma_1^{(th)} \simeq -0.0459$ .

### 3.2 The evolution of linear bias, $b(z)$

Here we briefly present the model that we use to trace the evolution of the linear bias factor, which reflects the relation between the overdensities of luminous and of dark matter [46, 47]. We remind the reader that biasing is considered to be statistical in nature with galaxies and clusters being identified as high peaks of an underlying, initially Gaussian, random density field. The usual paradigm is of a linear and scale-independent bias, defined as the ratio of density perturbations in the mass-tracer field to those of the underline total matter field:  $b = \delta_{tr}/\delta_m$ <sup>2</sup>.

In this analysis we use the bias evolution model of [29, 49]. This generalized model is based on the linear perturbation theory and the Friedmann-Lemaitre solutions of the cosmological field equations. It is valid for any DE model (scalar or geometrical) and it is given by:

$$b(z) = 1 + \frac{b_0 - 1}{D(z)} + C_2 \frac{\mathcal{J}(z)}{D(z)} \quad (3.18)$$

---

<sup>2</sup>We would like to point that up to galaxy cluster scales the fluctuations of the metric do not introduce a significant scale dependence in the growth factor [48] and in the linear bias [29].

with

$$\mathcal{J}(z) = \int_0^z \frac{(1+y)}{E(y)} dy. \quad (3.19)$$

The constants  $b_0$  (the bias at the present time) and  $C_2$  depend on the host dark matter halo mass, as we have verified using  $\Lambda$ CDM N-body simulations (see [29]), and are given by:

$$b_0(M_h) = 0.857 \left[ 1 + \left( C_m \frac{M_h}{10^{14} h^{-1} M_\odot} \right)^{0.55} \right] \quad (3.20)$$

$$C_2(M_h) = 1.105 \left( C_m \frac{M_h}{10^{14} h^{-1} M_\odot} \right)^{0.255}, \quad (3.21)$$

where  $C_m = \Omega_{m0}/0.27$ .

### 3.3 CDM Power Spectrum, $P(k)$

The CDM power spectrum is given by  $P(k) = P_0 k^n T^2(k)$ , where  $T(k)$  is the CDM transfer function and  $n \simeq 0.9671$  following the recent reanalysis of the Planck data by Spergel et al. [7]. Regarding  $T(k)$ , we use two different functional forms namely, that of Bardeen et al. [47] and of Eisenstein & Hu [50].

The [47] is given by:

$$T(k) = C_q \left[ 1 + 3.89q + (16.1q)^2 + (5.46q)^3 + (6.71q)^4 \right]^{-1/4} \quad (3.22)$$

where  $C_q = \frac{\ln(1+2.34q)}{2.34q}$  and  $q \equiv \frac{k}{\Gamma}$ . Here  $\Gamma$  is the shape parameter, given according to [51] as:

$$\Gamma = \Omega_{m0} \tilde{h} \exp(-\Omega_{b0} - \sqrt{2\tilde{h}} \Omega_{b0}/\Omega_{m0}). \quad (3.23)$$

The value of  $\Gamma$ , which is kept constant throughout the model fitting procedure, is estimated using the Planck results of Spergel et al. [7]<sup>3</sup> namely,  $\Omega_{b0} = 0.022197\tilde{h}^{-2}$ ,  $\tilde{h} = 0.68$  and  $\Omega_{m0} = 0.302$ . The alternative transfer function used is that of [50]:

$$T(k) = \frac{L_0}{L_0 + C_0 q^2} \quad (3.24)$$

where  $L_0 = \ln(2e + 1.8q)$ ,  $e = 2.718$  and  $C_0 = 14.2 + \frac{731}{1+62.5q}$ .

Also, the rms fluctuations of the linear density field on mass scale  $M_h$  is:

$$\sigma(M_h, z) = \left[ \frac{D^2(z)}{2\pi^2} \int_0^\infty k^2 P(k) W^2(kR) dk \right]^{1/2}, \quad (3.25)$$

where  $W(kR) = 3(\sin kR - kR \cos kR)/(kR)^3$  and  $R = (3M_h/4\pi\rho_0)^{1/3}$  with  $\rho_0$  denotes the mean matter density of the universe at the present time ( $\rho_0 = 2.78 \times 10^{11} \Omega_{m0} h^2 M_\odot \text{Mpc}^{-3}$ ). To this end, the normalization of the power spectrum is given by:

$$P_0 = 2\pi^2 \sigma_8^2 \left[ \int_0^\infty T^2(k) k^{n+2} W^2(kR_8) dk \right]^{-1} \quad (3.26)$$

---

<sup>3</sup>We use the Planck priors provided by Spergel et al. [7] in order to avoid possible systematics on the cosmological parameters which are related to the problematic (according to Spergel et al.) 217GHz×217GHz detector. However, at the end of the analysis we provide results based on the Planck results of Ade et al. [6].



**Table 2:** Results in the  $(\Omega_{m0}, \gamma, M_h, n_{\text{eff}})$  parameter space for the different  $T(k)$  and  $\sigma_8$ .

| $T(k)$  | $\Omega_{m0}$          | $\gamma$               | $M_h/10^{13} M_\odot$ | $n_{\text{eff}}$        | $\chi^2_{t,\text{min}}/df$ |
|---|------------------------|------------------------|-----------------------|-------------------------|----------------------------|
| $\sigma_8 = 0.797 (0.30/\Omega_{m0})^{0.26}$ [52] |                        |                        |                       |                         |                            |
| Hu  | $0.29 \pm 0.01$        | $0.56 \pm 0.05$        | $1.90 \pm 0.10$       | $0.10 \pm 0.20$         | 16.36/23                   |
| Bardeen   | $0.29 \pm 0.01$        | $0.56 \pm 0.10$        | $1.80 \pm 0.30$       | $-0.10^{+0.30}_{-0.10}$ | 16.56/23                   |
| $\sigma_8 = 0.818 (0.30/\Omega_{m0})^{0.26}$ [7]  |                        |                        |                       |                         |                            |
| Hu  | $0.29^{+0.03}_{-0.02}$ | $0.58^{+0.02}_{-0.06}$ | $1.70 \pm 0.20$       | $0.30 \pm 0.20$         | 15.90/23                   |
| Bardeen   | $0.29^{+0.02}_{-0.03}$ | $0.56 \pm 0.10$        | $1.60 \pm 0.4$        | $0.0^{+0.10}_{-0.20}$   | 16.13/23                   |

where  $\sigma_8 \equiv \sigma(R_8, 0)$  is the rms mass fluctuation on  $R_8 = 8h^{-1}$  Mpc scales and for which we use separately either of the two following parametrizations:

$$\sigma_8 = \begin{cases} 0.818 \left( \frac{0.30}{\Omega_{m0}} \right)^{0.26}, & \text{Spergel et al. [7]} \\ 0.797 \left( \frac{0.30}{\Omega_{m0}} \right)^{0.26}, & \text{Hajian et al. [52].} \end{cases} \quad (3.27)$$

Finally, we would like to stress that we have taken into account the non-linear corrections by using the corresponding fitting formula introduced by [53], for the  $\Lambda$ CDM model (see also [54, 55]). In their fitting formula there is one relatively free parameter, which is the slope of the power spectrum at the relevant scales, because the CDM power spectrum curves slowly and thus it varies as a function of scale according to:  $n_{\text{eff}} = d \ln P / d \ln k$ .

#### 4. Fitting Theoretical Models to the data

In this section we implement a standard  $\chi^2$  minimization statistical analysis in order to provide constraints either in the  $(\Omega_{m0}, \gamma)$  parameter space, or for  $\gamma(z)$ . An important ingredient that is necessary in Eq.(3.1), in order to relate the spatial to the angular two-point correlation functions, is the tracer redshift distribution. For the LRGs we use an analytic model of their photometric redshift distribution, which we then insert in Eq.(3.1). The model redshift distribution is given by fitting the following useful formula to the data:

$$\frac{dN}{dz} \propto \left( \frac{z}{z_\star} \right)^{(a+2)} e^{-\left( \frac{z}{z_\star} \right)^\beta}. \quad (4.1)$$

We obtain the relevant parameters by fitting the data of the redshift distribution to the above formula:

$$(a, \beta, z_\star) = (-15.53, -8.03, 0.55) \quad (4.2)$$

where  $z_\star$  is the characteristic depth of the subsample studied. In Fig.1, we present the estimated normalized redshift distribution  $(\frac{1}{N} \frac{dN}{dz})$  and the corresponding continuous fit provided by Eq.(4.1).

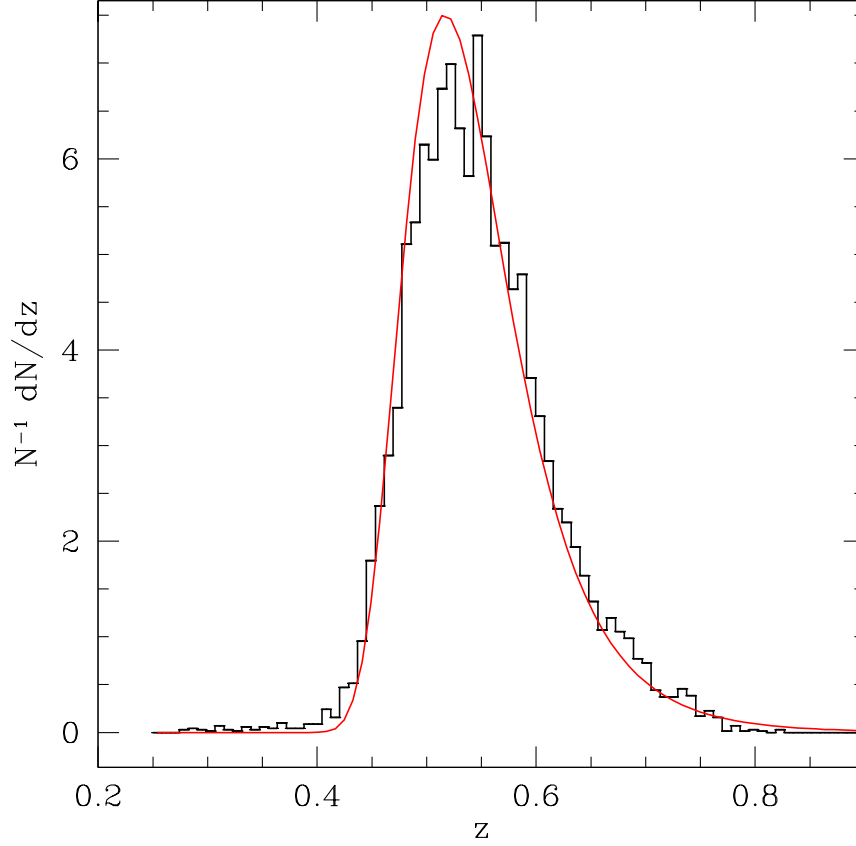


**Figure 1:** The normalized photometric redshift distribution of the 2SLAQ LRG galaxies. The red continuous line is its corresponding best fit according to Eq.(4.1).

We are now set to compare the measured 2SLAQ LRGs and growth functions with the predictions of different spatially flat  $\Lambda$  cosmological models. To this end we use the standard  $\chi^2$ -minimization procedure, which in our case it is defined as follows:

(1) For the LRG clustering cosmological probe:

$$\chi_{\text{LRGs}}^2(\mathbf{p}_1, \mathbf{p}_2) = \sum_{i=1}^{11} \frac{[w_{\text{th}}(\theta_i, \mathbf{p}_1, \mathbf{p}_2) - w_{\text{obs}}(\theta_i)]^2}{\sigma_i^2} . \quad (4.3)$$

where the expected theoretical ACF ( $w_{\text{th}}$ ) is given by Eq.(3.6) and  $\sigma_i$  is the observed ACF  $1\sigma$  uncertainty, and

(2) for the growth-rate cosmological probe:

$$\chi_{\text{gr}}^2(\mathbf{p}_1) = \sum_{i=1}^{16} \left[ \frac{C_f(z_i, \mathbf{p}_1) f\sigma_{8,\text{obs}}^{\text{Ref}}(z_i) - f\sigma_8(z_i, \mathbf{p}_1)}{C_f(z_i, \mathbf{p}_1) \sigma_i^{\text{Ref}}} \right]^2 \quad (4.4)$$

where  $\sigma_i^{\text{Ref}}$  is the observed  $1\sigma$  uncertainty, while  $C_f$  is given in Eq.(2.1), and the theoretical growth-rate is given by:

$$f\sigma_8(z, \mathbf{p}_1) = \sigma_8 D(z) \Omega_m(z)^{\gamma(z)} . \quad (4.5)$$

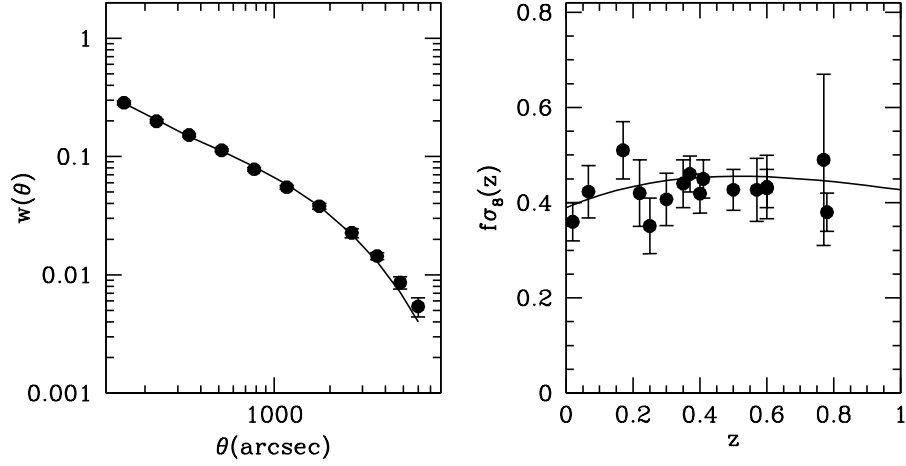


**Figure 2:** *Left Panel:* Comparison of the observed (solid points) and theoretical angular correlation function. *Right Panel:* Comparison of the observed (solid points) and theoretical evolution of the growth rate  $f(z)\sigma_8(z)$ . In order to obtain the theoretical curve we use  $(\Omega_{m0}, \gamma) = (0.29, 0.56)$  (for more details see section 4.1).

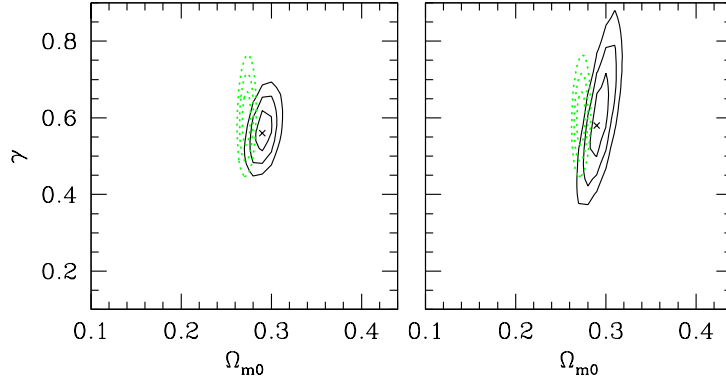


**Figure 3:** Likelihood contours for  $\Delta\chi^2 = \chi_t^2 - \chi_{t,\min}^2$  equal to 2.32, 6.18 and 11.83, corresponding to  $1\sigma$ ,  $2\sigma$  and  $3\sigma$  confidence levels, in the  $(\Omega_{m0}, \gamma)$  plane using the Eisenstein & Hu [50] transfer function and the [29, 49] bias model. *Left Panel:* The joint likelihood contours correspond to Hajian et al. [52] power spectrum normalization. *Right Panel:* The contours here correspond to  $\sigma_8$  provided by Spergel et al. [7]. The best fit solutions are represented by the crosses. Note that using the Bardeen et al. [47] transfer function we find almost the same results within  $1\sigma$  errors. Finally, the green dotted curves are the SNIa/BAOs/CMB<sub>shift</sub>/ $f\sigma_8$  joint likelihood contours provided by [56].

The vectors  $\mathbf{p}_1$  and  $\mathbf{p}_2$  provide the free parameters that enter in deriving the theoretical expectations. The "cosmo-gravity"  $\mathbf{p}_1$  vector contains those free parameters which are related to the expansion and gravity. For the case of constant  $\gamma$  it is defined as:  $\mathbf{p}_1 =$

$(\Omega_{m0}, \gamma, \sigma_8)$ , and for the case of evolving  $\gamma$ , as:  $\mathbf{p}_1 = (\Omega_{m0}, \gamma_0, \gamma_1, \sigma_8)$ . The  $\mathbf{p}_2 = (M_h, n_{\text{eff}})$  vector is associated with the environment of the dark matter halo in which the extragalactic mass tracers (in our case LRGs galaxies) live.

Since we wish to perform a joint likelihood analysis of the two cosmological probes and since likelihoods are defined as  $\mathcal{L} \propto \exp(-\chi^2/2)$ , one has that the joint likelihood is:

$$\mathcal{L}_t(\mathbf{p}_1, \mathbf{p}_2) = \mathcal{L}_{\text{LRGs}}(\mathbf{p}_1, \mathbf{p}_2) \times \mathcal{L}_{\text{gr}}(\mathbf{p}_1), \quad (4.6)$$

which is equivalent to:

$$\chi_t^2(\mathbf{p}_1, \mathbf{p}_2) = \chi_{\text{LRGs}}^2(\mathbf{p}_1, \mathbf{p}_2) + \chi_{\text{gr}}^2(\mathbf{p}_1). \quad (4.7)$$

Based on the above we will provide our results for each free parameter that enters in the two  $\mathbf{p}_{1,2}$  vectors. Note that the uncertainty of each fitted parameter will be estimated after marginalizing one parameter over the other, providing as its uncertainty the range for which  $\Delta\chi^2(\leq 1\sigma)$ . Such a definition, however, may hide the extent of a possible degeneracy between the fitted parameters and thus it is important to visualize the solution space, as indicated in the relevant contour figures.

As a further consistency check we have used the inverse of the Fisher matrix, the covariance matrix, but we find similar uncertainties to those provided by the marginalization method, most probably due to the fact that the 1, 2 and  $3\sigma$  solution space contours are symmetric and the axes of symmetry are parallel to the  $\mathbf{p}_{1,2}$  vectors. Since the errors of the Fisher matrix approach are symmetric by definition, we have decided to use the marginalization approach.

In the left panel of Fig. 2, we present the observed  $w(\theta)$  for the 2SLAQ LRGs (left panel), with the best fit model of the angular correlation function provided by Eq.(3.6) and the minimization procedure discussed above. In the right panel of Fig. 2, we plot the growth data (solid points) as collected by Basilakos et al. (see [57] and references therein) with the estimated (solid line) growth rate function,  $f(z)\sigma_8(z)$  (for more details see the discussion section 4.1).

#### 4.1 Constraints on $(\Omega_{m0}, \gamma)$

In our analysis we have set  $\sigma_8$  based on Eq.(3.27) and thus the cosmogravity vector contains only two independent free parameters, namely  $\mathbf{p}_1 = (\Omega_{m0}, \gamma)$ . Thus, we have four free parameters in total. We sample the various parameters as follows: the matter density  $\Omega_{m0} \in [0.01, 1]$  in steps of 0.01; the growth index  $\gamma \in [0.1, 1.0]$  in steps of 0.01, the parent dark matter halo (for the LRGs)  $M_h/10^{13}h^{-1}M_\odot \in [1, 2.5]$  and the slope of the power spectrum  $n_{\text{eff}} \in [-0.5, 1.0]$  in steps of 0.1.

In Table 2 we present our resulting parameter constraints separately for the case of the Hajian et al. [52] and the Spergel et al. [7] power spectrum normalizations respectively (see Eq.(3.27)), as well as for the two different CDM transfer functions used.

A first general result is that the two transfer functions used provide very similar cosmogravity results within  $1\sigma$  errors. Therefore, in the rest of the paper we utilize the Eisenstein & Hu [50] transfer function. Secondly, we would like to mention that the  $\chi_{t,\text{min}}^2$  for the Hajian et al. [52] normalization, results in a reduced value of  $\chi_{t,\text{min}}^2/df \sim 16.36/23$  while the corresponding  $\chi_{t,\text{min}}^2/df$  value for the Spergel et al. [7] is  $\sim 15.90/23$ . In Figure 3 we present the  $1\sigma$ ,  $2\sigma$  and  $3\sigma$  confidence contours in the  $(\Omega_{m0}, \gamma)$  plane for both  $\sigma_8$  normalization ([7]: right panel and [52]: left panel). These results are based on the transfer

**Table 3:** Literature growth results for the  $\Lambda$ CDM cosmological model. The last line corresponds to our results. Similar to [57] results can be also found in [56].

| Data used   | $\Omega_{m0}$             | $\gamma$                  | References       |
|---|---------------------------|---------------------------|------------------|
| galaxy data from 2dFGRS                                     | $0.30 \pm 0.02$           | $0.60^{+0.40}_{-0.30}$    | [58]             |
| old $f(z)$ growth data                                      | 0.30                      | $0.674^{+0.195}_{-0.169}$ | [17]             |
| old $f(z)$ growth data                                      | $0.273 \pm 0.015$         | $0.64^{+0.17}_{-0.15}$    | [20]             |
| X-ray cluster luminosity function+ $f_{gas}$                | $0.214^{+0.036}_{-0.041}$ | $0.42^{+0.20}_{-0.16}$    | [59]             |
| WMAP+SNiA+MCMC  | 0.25                      | $0.584 \pm 0.112$         | [60]             |
| old+new $f(z)$ growth data                                  | $0.273 \pm 0.011$         | $0.586^{+0.079}_{-0.074}$ | [45]             |
| $f\sigma_8$ growth data                                     | $0.259 \pm 0.045$         | $0.619 \pm 0.054$         | [61]             |
| $f\sigma_8$ growth data                                     | 0.273                     | $0.602 \pm 0.055$         | [62]             |
| old+new $f(z)$ growth data                                  | 0.273                     | $0.58 \pm 0.04$           | [63]             |
| $f\sigma_8$ growth data+(SNiA, BAOs, CMB <sub>shift</sub> ) | $0.272 \pm 0.003$         | $0.597 \pm 0.046$         | [56, 57]         |
| CMASS DR9+ other $f\sigma_8$                                | $0.308 \pm 0.022$         | $0.64 \pm 0.05$           | [64]             |
| cl+CMB+gal+SNiA+BAO   | $0.284 \pm 0.012$         | $0.618 \pm 0.062$         | [65]             |
| Lensing + $f\sigma_8$ growth data                           | $0.256 \pm 0.023$         | $0.52 \pm 0.09$           | [66]             |
| CMB+clustering of Baryon Oscillation Spec. Survey           | $0.30 \pm 0.01$           | $0.69 \pm 0.15$           | [67]             |
| $f\sigma_8$ growth data+(SNiA, BAOs, CMB <sub>CAMB</sub> )  | $0.298^{+0.027}_{-0.023}$ | $0.675^{+0.18}_{-0.16}$   | [68]             |
| <b>Clustering of LRGs+ growth data</b>                      | $0.29 \pm 0.01$           | $0.56 \pm 0.05$           | <b>Our study</b> |

function of Ref.[50]. As it can also be seen from Table 2,  $\Omega_{m0} = 0.29 \pm 0.01$ , which is in a very good agreement with the Planck [7] results, while the derived value of  $\gamma = 0.56 \pm 0.05$  coincides with the theoretically expected  $\Lambda$ CDM value. Inserting  $\Omega_{m0} = 0.29$  into the second branch of Eq.(3.27) we obtain  $\sigma_8 \simeq 0.804$ . The aforementioned environmental vector is  $\mathbf{p}_2 = ((1.90 \pm 0.2) \times 10^{13} h^{-1} M_\odot, 0.10 \pm 0.20)$ . It is interesting to mention, that our derived host DM halo mass is consistent with that of Sawangwit et al. [35], namely  $M_h = (2.1 \pm 0.1) \times 10^{13} h^{-1} M_\odot$ . Alternatively, considering the Planck prior [7] of  $\Omega_{m0} = 0.30$  and minimizing with respect to  $\gamma$  and  $\mathbf{p}_2 = (M_h, n_{\text{eff}})$  we find  $\gamma = 0.56 \pm 0.05$  and  $\mathbf{p}_2 = ((2.0 \pm 0.10) \times 10^{13} h^{-1} M_\odot, 0.30 \pm 0.20)$  with  $\chi^2_{t,\text{min}}/df \sim 16.52/24$ .

With respect to other recent studies, our best fit values of  $\gamma$  are in agreement, within  $1\sigma$  errors, to that of [56] (see also [57]) who found  $\gamma = 0.597 \pm 0.046$ , using a combined statistical analysis of expansion and growth data (SNiA/BAOs/CMB<sub>shift</sub>/ $f\sigma_8$ ). However, our joint  $\Omega_{m0}$  value is somewhat greater (within  $\sim 1.8\sigma$  uncertainty), from the derived value of [56],  $\Omega_{m0} = 0.272 \pm 0.003^4$ . For comparison, in Figure 3 we also display the combined  $(\Omega_{m0}, \gamma)$  likelihood contours (see green dotted lines) of [56]. It is evident that the combined analysis of the growth data with the LRGs clustering provides strong constraints on the growth parameter  $\gamma$ , which implies that this method works equally well with that of the joint SNiA/BAOs/CMB<sub>shift</sub>/ $f\sigma_8$ .

In order to appreciate the great effort in the recent years to estimate jointly  $\Omega_{m0}$  and  $\gamma$  and the relative strength and precision of the different methods, we present a summary of relevant literature results in Table 3. It appears unavoidable to conclude that current data favor, within a  $1\sigma$  uncertainty, the theoretically predicted value of  $\gamma_\Lambda^{(th)} \simeq 6/11$ . Secondly, the quality and quantity of the cosmological and dynamical (growth and the like) data as well as methodologies have greatly improved in recent years. For example, since the first

<sup>4</sup>Nesseris et al. [56] imposed  $\sigma_8 = 0.80$ .

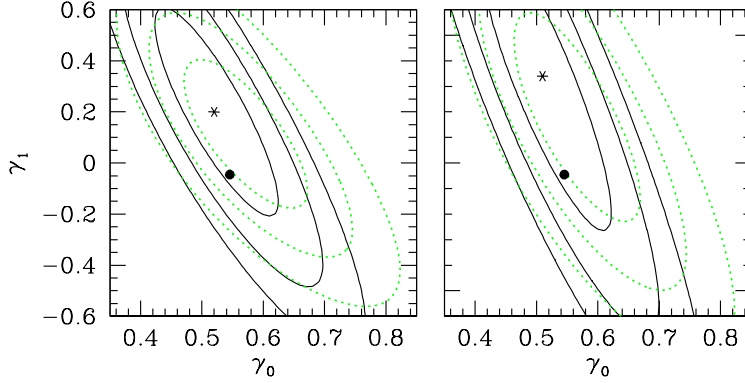


**Figure 4:** The joint 2SLAQ (LRGs) galaxy  $w(\theta)$  and  $f\sigma_8$  likelihood contours (solid curves) in the  $(\gamma_0, \gamma_1)$  plane (using  $\Omega_{m0} = 0.30$  and  $\sigma_8 = 0.797$ ). The left and right panels show the results based on the  $\Gamma_1$  and  $\Gamma_2$  parametrizations respectively. The crosses correspond to the best fit parameters. We also show the theoretical  $\Lambda$ CDM  $(\gamma_0^{(th)}, \gamma_1^{(th)})$  values (solid points) given in section 4.1. Finally, the green dotted curves are the SNIa/BAOs/CMB<sub>shift</sub>/ $f\sigma_8$  joint likelihood contours provided by [56].

**Table 4:** Literature  $(\gamma_0, \gamma_1)$  constraints. The bold phase lines correspond to the present analysis.

| Parametrization Model                                    | $\gamma_0$                | $\gamma_1$                | Reference        |
|--|---------------------------|---------------------------|------------------|
| $\Gamma_1 : \gamma(z) = \gamma_0 + \gamma_1 z$           | $0.77 \pm 0.29$           | $-0.38 \pm 0.85$          | [17]             |
|  | 0.774                     | -0.556                    | [21]             |
|  | $0.49^{+0.12}_{-0.11}$    | $0.305^{+0.345}_{-0.318}$ | [45]             |
|  | $0.48 \pm 0.07$           | $0.32 \pm 0.20$           | [63]             |
|  | $0.40^{+0.086}_{-0.080}$  | $0.603 \pm 0.241$         | [62]             |
|  | $0.567 \pm 0.066$         | $0.116 \pm 0.19$          | [56, 57]         |
|  | $0.520 \pm 0.04$          | $0.02 \pm 0.11$           | <b>Our study</b> |
| $\Gamma_2 : \gamma(z) = \gamma_0 + \gamma_1 z / (1 + z)$ | $0.92^{+1.56}_{-1.26}$    | $-1.49^{+6.86}_{-6.08}$   | [69]             |
|  | $0.461^{+0.12}_{-0.11}$   | $0.513^{+0.448}_{-0.414}$ | [45]             |
|  | $0.46 \pm 0.09$           | $0.55 \pm 0.36$           | [63]             |
|  | $0.345^{+0.085}_{-0.080}$ | $1.006 \pm 0.314$         | [62]             |
|  | $0.561 \pm 0.068$         | $0.183 \pm 0.26$          | [56, 57]         |
|  | $0.560 \pm 0.03$          | $-0.10 \pm 0.11$          | <b>Our study</b> |

measurement of [58], the error budget of the growth index has been decreased by one order of magnitude with respect to best fit value of the current work. It is also important to note that using only the combine basic properties of the large scale structures (ACF of 2SLAQ LRGs and growth data) we have managed to significantly reduce the growth index uncertainty, namely  $\sigma_\gamma/\gamma \sim 9\%$  and thus producing one of the strongest (to our knowledge) existing joint constraints on  $\gamma$ .

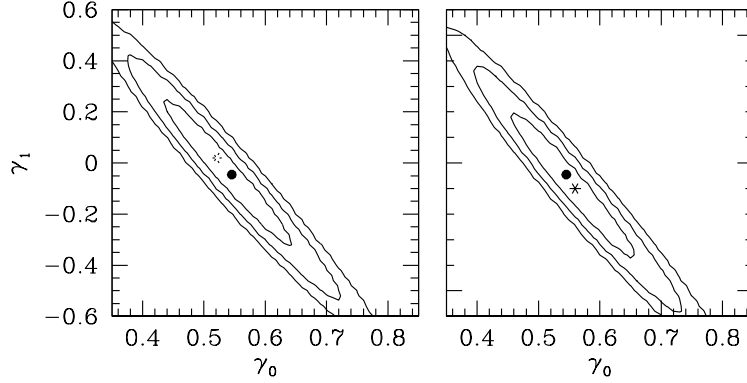


**Figure 5:** The Likelihood contours in the  $(\gamma_0, \gamma_1)$  plane (see caption of Fig. 4 for definitions). Here the normalization of the power spectrum is given by Eq.(4.8).

#### 4.2 Constraints on $\gamma(z)$

In this section we perform a consistent minimization procedure in the  $(\gamma_0, \gamma_1)$  parameter space. Following the considerations discussed in the previous section and for the sake of simplicity the "cosmo-gravity" vector becomes  $\mathbf{p}_1 = (0.30, \gamma_0, \gamma_1, \sigma_8)$ , where we have marginalized the overall likelihood analysis over the LRG environmental vector  $(M_h, n_{\text{eff}}) = (2.0 \times 10^{13} h^{-1} M_\odot, 0.30)$ . We sample  $\gamma_0 \in [0.35, 0.85]$  in steps of 0.01 and  $\gamma_1 \in [-0.6, 0.6]$  in steps of 0.01. Note, that as in [56] we first use a constant  $\sigma_8$ , namely  $\sigma_8 = 0.797$ .

In Fig.4 we plot the results of our statistical analysis in the  $(\gamma_0, \gamma_1)$  plane for the Eisenstein & Hu [50] transfer function, since we have verified that using Bardeen et al. [47] transfer function we get similar contours. The left panel shows the results based on the  $\Gamma_1$  parametrization while the right panel those of the  $\Gamma_2$  parametrization. Our contours are in agreement with those of [56] (see green dashed curves in Fig.4) which implies that practically our likelihood analysis provides similar results with those of SNIa/BAOs/CMB<sub>shift</sub>/ $f\sigma_8$ .

The theoretical  $(\gamma_0^{(th)}, \gamma_1^{(th)})$   $\Lambda$ CDM values (see above) are indicated by the solid points while the stars represent our best fit values which are:

- for the  $\Gamma_1$  parametrization we have  $\chi^2_{t,\text{min}}/df = 16.0/25$ ,  $\gamma_0 = 0.52 \pm 0.08$ ,  $\gamma_1 = 0.20 \pm 0.32$ .
- for the  $\Gamma_2$  parametrization: similarly, we obtain  $\chi^2_{t,\text{min}}/df = 15.87/25$ ,  $\gamma_0 = 0.51 \pm 0.08$ ,  $\gamma_1 = 0.34^{+0.26}_{-0.46}$ .

Obviously, the  $\gamma_1$  parameter is not constrained by this analysis, which is however also the case for the joint SNIa/BAOs/CMB<sub>shift</sub>/ $f\sigma_8$  analysis [56]. This effect is partially attributed to the constant  $\sigma_8$ . Therefore, we attempt to alleviate this by additionally treating the  $\sigma_8$  prior properly along the  $\gamma$ -chain. Following the normalization procedure of

[70] we rescale the value of  $\sigma_8$  by

$$\sigma_{8,\gamma} = \sigma_8 \frac{\delta_m(1, \gamma_0, \gamma_1)}{\delta_m(1, \gamma_0^{(th)}, \gamma_1^{(th)})} . \quad (4.8)$$

where  $\sigma_8 = 0.797$  and  $\delta_m(a, \gamma)$  is given by Eq.(3.14). We repeat our statistical analysis by using  $\sigma_{8,\gamma}$  in the "cosmo-gravity" vector and we find:

- for the  $\Gamma_1$  parametrization:  $\gamma_0 = 0.52 \pm 0.04$ ,  $\gamma_1 = 0.02 \pm 0.11$  with  $\chi_{t,\min}^2/df = 17.5/25$ .
- for the  $\Gamma_2$  parametrization:  $\gamma_0 = 0.56 \pm 0.03$ ,  $\gamma_1 = -0.10 \pm 0.11$  with  $\chi_{t,\min}^2/df \simeq 17.3/25$ .

It is evident that the predicted  $\Lambda$ CDM  $(\gamma_0^{(th)}, \gamma_1^{(th)})$  values of both parametrizations are close to the best fit parameters (see solid points in Fig. 5). Finally, comparing the contours of Fig.5 with literature results (for the corresponding Refs. see Table 3) we find that indeed we have managed to reduce significantly the area of  $\gamma_0 - \gamma_1$  contours, increasing the Figure of Merit by  $\sim 30\%$ , with respect to that of the constant  $\sigma_8$  analysis (see Fig. 4). Also, in Table 4, one may see a more compact presentation of our results including literature best fit  $(\gamma_0, \gamma_1)$  values.

### 4.3 Using the priors provided by the Planck team

In order to complete the current study we repeat our analysis by using those priors derived originally by the Planck team [6], namely

$$(\Omega_{b0}, \tilde{h}, n, \sigma_8) = (0.02207\tilde{h}^{-2}, 0.674, 0.9616, \sigma_8)$$

with  $\sigma_8 = 0.87(0.27/\Omega_{m0})^{0.3}$ . Since, we have found that the results remain mostly unaffected by using the two different forms of  $T(k)$ , we use here the form of Ref.[50]. In brief we find:

- the overall likelihood function peaks at  $(\Omega_{m0}, \gamma) = (0.29_{-0.03}^{+0.02}, 0.56_{-0.06}^{+0.02})$  with  $\chi_{t,\min}^2/df \simeq 15/24$ . The corresponding environmental vector is  $\mathbf{p}_2 = (1.40 \pm 0.1 \times 10^{13} h^{-1} M_\odot, 0.4 \pm 0.20)$ . If we impose  $\Omega_{m0} = 0.315$  then we find  $\gamma = 0.58_{-0.10}^{+0.02}$ ,  $\mathbf{p}_2 = (1.60 \pm 0.1 \times 10^{13} h^{-1} M_\odot, 0.8 \pm 0.10)$  with  $\chi_{t,\min}^2/df \simeq 17.1/25$ .

Furthermore, using the latter  $\Omega_{m0}$  and  $\mathbf{p}_2$  we obtain:

- in the case of  $\Gamma_1$  parametrization:  $\chi_{t,\min}^2/df = 18/25$ ,  $\gamma_0 = 0.55 \pm 0.04$ ,  $\gamma_1 = -0.06 \pm 0.12$ .
- in the case of  $\Gamma_2$  parametrization:  $\chi_{t,\min}^2/df = 17.8/25$ ,  $\gamma_0 = 0.55 \pm 0.04$ ,  $\gamma_1 = -0.08 \pm 0.12$ . Notice, that for both  $\gamma(z)$  parametrizations we utilize Eq.(4.8) as far as the variable  $\sigma_{8,\gamma}$  is concerned.



## 5. Conclusions

In the epoch of intense cosmological studies aimed at testing the validity of general relativity on extragalactic scales, it is very important to minimize the amount of priors needed to successfully complete such an effort. One such prior is the growth index and its measurement at the  $\sim 1\%$  accuracy level has been proposed as a necessary step for checking possible departures from general relativity at cosmological scales [30]. Therefore, it is of central importance to have independent determinations of  $\gamma$ , because this will help to control the systematic effects that possibly affect individual methods and tracers of the growth of matter perturbations.

In this study we use the basic large scale structure properties such as the clustering of the 2SLAQ Luminous Red Galaxies together with the growth rate of clustering provided by the various galaxy surveys in order to constrain the growth index of matter perturbations. The results of the two analyzes are used in a joint likelihood fitting procedure which helps to reduce the parameter uncertainties. The outcome constraints are:  $(\Omega_{m0}, \gamma) = (0.29 \pm 0.01, 0.56 \pm 0.05)$ , which are the strongest (to our knowledge) joint constraints appearing in the literature. Also, we check that our growth results are quite robust against the choice of the transfer function of the power spectrum and the Planck priors which are available in the literature [6, 7].

Finally, considering a time varying growth index:  $\gamma(z) = \gamma_0 + \gamma_1 X(z)$ , with  $X(z) = z$  or  $X(z) = z/(1+z)$  we find, as all similar studies, that  $\gamma_1$  and  $\gamma_0$  are somehow degenerate. However, based on the joint statistical analysis we have managed to put tighter constraints on  $\gamma_0$ . Although, we have reduced significantly the  $\gamma_1$  uncertainty with respect to previous studies, the corresponding error bars remain quite large. Future, dynamical data are expected to improve even further the relevant constraints (especially on  $\gamma_1$ ) and thus the validity of GR on cosmological scales will be effectively tested.

## Acknowledgments

We are greatly thankful to Dr. S. Nesseris for providing us with an electronic version of their growth  $\Omega_{m0} - \gamma$  and  $\gamma_0 - \gamma_1$  contours. AP acknowledges financial support under the Academy of Athens: *Fellowship for Astrophysics* grant 2005-49878. SB also acknowledges support by the Research Center for Astronomy of the Academy of Athens in the context of the program “*Tracing the Cosmic Acceleration*”.

## References

- [1] M. Hicken et al., *Astrophys. J.*, **700**, 1097 (2009)
- [2] E. Komatsu et al., *Astrophys. J. Supp.*, **192**, 18 (2011)
- [3] C. Blake et al., *Mon. Not. Roy. Soc.*, **418**, 1707 (2011)
- [4] G. Hinshaw et al., *Astrophys. J. Supp.*, **208**, 19 (2013)
- [5] O. Farooq, D. Mania and B. Ratra, *Astrophys. J.*, **764**, 138 (2013).
- [6] P. A. R. Ade et al., (Planck Collaboration), arXiv:1303.5076 (2013)
- [7] D. Spergel, R. Flauger and R. Hlozek, arXiv:1312.3313 (2013)
- [8] E. J. Copeland, M. Sami and S. Tsujikawa, *Int. J. of Mod. Phys. D.*, **15**, 1753 (2006)

- [9] R. R. Caldwell and M. Kamionkowski, *Ann. Rev. Nucl. Part. Sci.*, **59**, 397 (2009)
- [10] L. Amendola and S. Tsujikawa, *Dark Energy: Theory and Observations*, Cambridge University Press, Cambridge UK (2010)
- [11] E. V. Linder, *Phys. Rev. D.*, **70**, 023511 (2004)
- [12] E. V. Linder and R. N. Cahn, *Astrop. Phys.*, **28**, 481 (2007)
- [13] H. Steigerwald, J. Bel and C. Marinoni, *JCAP*, **5**, 42, 2014
- [14] P. J. E. Peebles, “*Principles of Physical Cosmology*”, Princeton University Press, Princeton New Jersey (1993)
- [15] L. Wang and P. J. Steinhardt, *Astrophys. J.*, **508**, 483 (1998)
- [16] V. Silveira and I. Waga, *Phys. Rev. D.*, **50**, 4890 (1994)
- [17] S. Nesseris and L. Perivolaropoulos, *Phys. Rev. D.*, **77**, 023504 (2008)
- [18] G. Dvali, G. Gabadadze and M. Porrati, *Phys. Lett. B.*, **485**, 208 (2000)
- [19] H. Wei, *Phys. Lett. B.*, **664**, 1 (2008)
- [20] Y. Gong, *Phys. Rev. D.*, **78**, 123010 (2008)
- [21] X. Fu, P. Wu and H. Yu, *Phys. Lett. B*, **677**, 12 (2009)
- [22] R. Gannouji, B. Moraes and D. Polarski, *JCAP*, **2**, 34 (2009)
- [23] S. Tsujikawa, R. Gannouji, B. Moraes and D. Polarski, *Phys. Rev. D.*, **80**, 084044 (2009)
- [24] S. Basilakos and P. Stavrinos, *Phys. Rev. D.*, **87**, 043506 (2013)
- [25] T. Matsubara, *Astrophys. J.*, **615**, 573 (2004)
- [26] S. Basilakos and M. Plionis, *Mon. Not. Roy. Soc.*, **360**, L35 (2005)
- [27] S. Basilakos and M. Plionis, *Astrophys. J.*, **650**, L1 (2006)
- [28] M. Krumpe, T. Miyaji and A. L. Coil, *arXiv:1308.5976* (2013)
- [29] S. Basilakos, J. B. Dent, S. Dutta, L. Perivolaropoulos and M. Plionis, *Phys. Rev. D.*, **85**, 123501 (2012)
- [30] R. Bean, *American Astronomical Society Meeting Abstracts*, **223**, 341.05 (2014)
- [31] S. Nesseris and J. Garcia-Bellido, *JCAP*, **11**, 33 (2012)
- [32] M. J. Hudson and S. J. Turnbull, *Astrophys. J. Let.* **751**, 30 (2012)
- [33] F. Beutler, et al., *Mon. Not. Roy. Astron. Soc.*, **423**, 3430 (2012)
- [34] S. Basilakos, S. Nesseris and L. Perivolaropoulos, *Phys. Rev. D.*, **87**, 123529 (2013)
- [35] U. Sawangwit et al., *Mon. Not. Roy. Soc.*, **416**, 3033 (2011)
- [36] Y-S. Song and W.J. Percival, *J. Cosmol. Astropart. Phys.*, **10** (2009) 004
- [37] C. M. Cress and M. Kamionkowski, *Mon. Not. Roy. Soc.*, **297**, 486 (1998)
- [38] A. Lue, R. Scoccimarro and G. D. Starkman, *Phys. Rev. D.*, **69**, 124015 (2004)
- [39] H. F. Stabenau and B. Jain, *Phys. Rev. D.*, **74**, 084007 (2006)
- [40] P. J. Uzan, *Gen. Rel. Grav.*, **39**, 307 (2007)
- [41] S. Tsujikawa, K. Uddin and R. Tavakol, *Phys. Rev. D.*, **77**, 043007 (2008)
- [42] D. Polarski and R. Gannouji, *Phys. Lett. B.*, **660**, 439 (2008)

- [43] G. Ballesteros and A. Riotto, Phys. Lett. B. **668**, 171 (2008)
- [44] A. B. Belloso, J. Garcia-Bellido and D. Sapone, JCAP, **10**, 10 (2011)
- [45] S. Basilakos, Intern. Journal of Modern Physics D, **21**, 1250064 (2012)
- [46] N. Kaiser, Astrophys. J. L., **284**, L9 (1984)
- [47] J. M. Bardeen, J. R. Bond, N. Kaiser and A. S. Szalay, Astrophys. J., **304**, 15 (1986)
- [48] J. B. Dent, S. Dutta and L. Perivolaropoulos, Phys. Rev. D., **80**, 023514 (2009)
- [49] S. Basilakos, M. Plionis and A. Pouri, Phys. Rev. D., **83**, 123525 (2011)
- [50] D. J. Eisenstein and W. Hu, Astrophys. J., **496**, 605 (1998)
- [51] N. Sugiyama, Astrophys. J. Supp., **100**, 281 (1995)
- [52] A. Hajian, N. Battaglia, D. N. Spergel, J. R. Bond, C. Pfrommer and J. L. Sievers, JCAP, **11**, 64 (2013)
- [53] J. A. Peacock and S. J. Dodds, Mon. Not. Roy. Soc., **267**, 1020 (1994)
- [54] R. E. Smith et al., Mon. Not. Roy. Soc., **341**, 1311 (2003)
- [55] L. M. Widrow, P. J. Elahi, R. J. Thacker, M. Richardson and E. Scannapieco, Mon. Not. Roy. Soc., **397**, 1275 (2009)
- [56] S. Nesseris, S. Basilakos, E. N. Saridakis and L. Perivolaropoulos, Phys. Rev. D., **88**, 103010, (2013)
- [57] S. Basilakos, S. Nesseris and L. Perivolaropoulos, Phys. Rev. D., **87**, 123529 (2013)
- [58] C. di Porto and L. Amendola, Phys. Rev. D., **77**, 083508 (2008)
- [59] D. Rapetti, S. W. Allen, A. Mantz and H. Ebeling, Mon. Not. Roy. Soc., **406**, 1796 (2010)
- [60] L. Samushia, W. J. Percival and A. Raccanelli, Mon. Not. Roy. Soc., **420**, 2102 (2012)
- [61] M. J. Hudson and S. J. Turnbull, Astrophys. J. Lett., **751**, L30 (2012)
- [62] S. Basilakos and A. Pouri, Mon. Not. Roy. Soc., **423**, 3761 (2012)
- [63] S. Lee, arXiv: 1205.6304 (2012)
- [64] L. Samushia et al., Mon. Not. Roy. Soc., **429**, 1514 (2013)
- [65] D. Rapetti, C. Blake, S. W. Allen, A. Mantz, D. Parkinson and F. Beutler, Mon. Not. Roy. Soc., **432**, 973 (2013)
- [66] F. Simpson et al., Mon. Not. Roy. Soc., **429**, 2249 (2013)
- [67] A. G. Sanchez, et al., Mon. Not. Roy. Astron. Soc, **440**, 2692 (2014)
- [68] Xu, L., Phys. Rev. D., **88**, 084032 (2013)
- [69] J. Dossett, M. Ishak, J. Moldenhauer, Y. Gong, and A. Wang, JCAP, **4**, 22 (2010)
- [70] S. Basilakos, M. Plionis and J.A.S. Lima, Phys. Rev. D., **82**, 083517 (2010)